Proc. of the European Safety and Reliability Conference (ESREL 2026)
Edited by José C. Matos, Paulo B. Lourenço, Michael Beer, Daniel Oliveira, Edoardo Patelli, Hélder S. Sousa, Rui A. Silva and Monica Santamaria

Published by Research Publishing, Singapore.
doi: 10.3850/ESREL2026061419_esrel26-p26386-cd

Physics-Informed Graph Neural Networks for Stress Prediction in Welded Structures

Lukas Pürner

Chair of Artificial Intelligence in Mechanical Engineering, Hochschule München, Germany.
E-mail: lukas.puerner@proton.me

Maximilian Kling

Institute of Material- and Building Research IMB at Munich University of Applied Sciences, Hochschule München, Germany. E-mail: maximilian.kling@hm.edu

Marcin Hinz

Chair of Artificial Intelligence in Mechanical Engineering, Hochschule München, Germany.
E-mail: marcin.hinz@hm.edu

Klemens Rother

Institute of Material- and Building Research IMB at Munich University of Applied Sciences, Hochschule München, Germany. E-mail: klemens.rother@hm.edu

The reliable prediction of stresses in welded structures is crucial for fatigue assessment and safety design. Conventional numerical methods such as the Finite Element Method (FEM) provide accurate results but are computationally expensive, which limits their use in large-scale optimization. Graph Neural Networks (GNNs) offer a promising alternative as they can exploit the inherent graph structure of finite element meshes and enable much faster evaluation once trained.
In this work, we present a GNN model for stress prediction in welded components, with particular focus on the notch stress in weld seams, which are critical for fatigue life. A standard encoder–process–decoder GNN commonly used for stress prediction is compared to a physics-informed variant. The GNN is trained using FEM simulations that incorporate variations in the weld seam geometry, leading to substantial differences in the maximum notch stress. The proposed approach is applied to a butt joint and a fillet joint, representative of typical configurations found in welded structures.
The physics-informed model demonstrates improved performance in predicting the critical maximum stresses in weld seams, although its overall accuracy across the full stress distribution is slightly lower. Furthermore, an evaluation metric is introduced that specifically quantifies fatigue-relevant stresses, as these aspects are often not adequately captured by conventional evaluation metrics for artificial intelligence models. The proposed metric provides a more meaningful assessment of model performance in terms of structural integrity and fatigue safety.

Keywords: Graph Neural Networks, Stress prediction, Welded structures, Deep learning, Physics-informed machine learning.

1. Introduction

FEM simulations are widely employed for the simulation of real-world physical systems. Within the FEM framework, the governing equations of the underlying physics are reformulated into a variational form and subsequently discretized. This discretization is performed on a computational mesh, whose element quality and resolution directly influence the accuracy of the numerical solution (Kim et al. 2018). As the size and complexity of FEM models increase, this dependency leads to substantial computational costs and efficiency limitations. Recent advances in machine learning (ML) have demonstrated significant potential to match the predictive accuracy of conventional numerical solvers while substantially accelerating physics-based simulations (Herrman et al. 2024). ML-based approaches provide an alternative way to study structure–property relationships by combining large datasets from physics-based simulations with modern learning algorithms.

Since physical simulations operate on mesh-based discretizations that can be naturally represented as graphs, graph neural networks (GNNs) are particularly well suited as surrogate models (Hamilton et al. 2020, Pfaff et al. 2021). A mesh consists of nodes and edges, on which relevant physical quantities-such as displacements, stresses, and velocities are typically evaluated (Pfaff et al. 2021). Recent studies have used GNN models to predict stresses or displacements in mesh-based structures, with the networks trained on solutions obtained from FEM simulations. However, most existing work has focused primarily on overall predictive accuracy, rather than on the accurate prediction of stress quantities that are critical for lifetime assessment.

Therefore, this study implements a state-of-the-art encoder–processor–decoder graph neural network architecture and introduces a modified loss function designed to improve the prediction accuracy of lifetime-relevant stresses. The resulting model predicts nodal stress distributions for a given mesh structure. The structures investigated in this work are welded components, specifically a butt weld and a fillet weld. In addition, the generalization performance of the trained GNN models is evaluated.

2. Related work

There are several methods for performing stress prediction in mesh-based bodies, but GNNs have received increasing attention in recent years. A major advantage of GNNs is that, unlike convolutional neural networks, they do not operate on rectangular domains but graph structures, which is highly beneficial for numerical simulation methods that use complex mesh structures (Zhou et al. 2020). GNNs are often employed within an encoder–processor–decoder architecture (Battaglia et al., 2018). Using GNNs, it is also possible to construct time-dependent surrogate models, in which the mesh is adapted and remeshed at each time step (Pfaff et al. 2025; Heller et al. 2024).

In addition, several methods have been proposed to further enhance GNNs. For instance, Jin et al. (2023) introduces a neural operator approach in which the FEM mesh is remeshed to generate more uniform elements, thereby improving generalization capability. Other studies augment GNNs with physics-informed neural networks (PINNs) to guide the learning process more explicitly. In this context, Dalton et al. 2023 and Zhou et al. 2024 employ the principle of minimum potential energy and additional boundary conditions during training. In contrast, Boldani et al. 2022 incorporates the balance of linear momentum as prior information, with spatial derivatives computed directly on the mesh.

Other relevant studies specifically addressing stress prediction in mesh-based structures with GNNs include Yang et al. 2025, Shivaditya et al. 2023, Gulakala et al. 2022, Jelovica et al. 2024, Xia et al. 2025, Wu et al. 2024 and Wong et al. 2023.

3. Dataset generation

The FEM dataset used for training of the GNNs was generated using ANSYS Parametric Design Language. In this process, the geometries of the meshed bodies were systematically varied while the applied loading conditions were kept constant (see Fig. 1 and Table 1). The sideview of Fig. 1 was 20 mm extruded to create a 3D body.

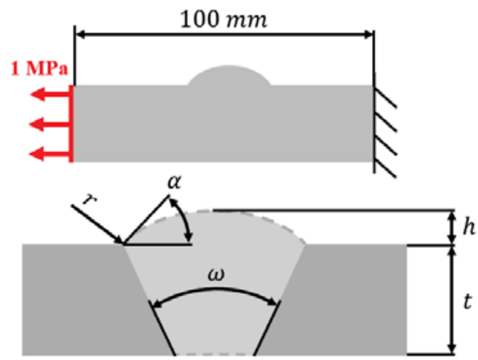

Fig. 1. Loading condition and geometry parameters for the butt weld geometry.

Table 1. Value ranges of the geometry parameters for the FEM-Simulations for the butt weld geometry.

Geometry parameter	Value range
Reference radius r	0.2 – 3.0 mm
Hight weld reinforcement h	0.1 – 0.3 mm
Plate thickness t	10 – 30 mm
Opening angle ω	30 – 60 deg
Weld flank angle α	40 – 60 deg

The dataset was then reduced to achieve uniform distribution of notch stresses in the weld transition region. This step is essential, as a bias in the notch stress distribution would otherwise lead to a corresponding bias in the prediction accuracy of the trained models. The final dataset for the butt-joint weld contained 247 FEM simulations.

The meshing of the FEM models is based on the notch stress approach, in which the sharp edge at the weld transition is replaced by a reference radius r (Heering et al. 2021). This modeling strategy results in numerically stable solutions, and for predefined reference radii, corresponding FAT classes are available, defining the allowable stress range for a given weld geometry at 2×10^6 load cycles. For dataset generation, the reference radius was systematically varied, resulting in a more complex and diverse dataset. Since meshing guidelines from Heering et al. 2021 specify a minimum number of elements in the reference radius, but meshing the whole body with such small elements would be computationally inefficient, two different element sizes were employed: a local weld element size in the reference radius and a global element size for the rest of the body. The two mesh parameters were selected to ensure overall high mesh quality for all geometries considered. The global element size was set to 1 mm, while the weld region was discretized using 32 elements per 360°. Linear hexahedral elements were used throughout, and a linear elastic material was assumed using a Young's modulus E = 210 GPa and a Poisson's ratio of ν = 0.3, which are typical values for structural steel. The resulting meshes typically contained between 100,000 and 200,000 nodes, with individual simulation runtimes ranging from approximately 30 to 60 seconds.

4. Graph neural network

4.1. *Preprocessing*

During the preprocessing stage, the FEM solutions are converted into a graph representation suitable for training the GNN models. To this end, node and edge features are constructed. The node features consist of the Cartesian coordinates x, y, and z as well as a binary indicator specifying whether a node is located on the boundary of the mesh, encoded using one-hot encoding. Consequently, the node feature matrix has a dimension of $N \times 5$, where N denotes the number of nodes in the corresponding graph.

The edge features are derived from the edge vector connecting two nodes and its norm. As a result, the edge feature matrix has a dimension of $E \times 4$, where E represents the number of edges in the graph. In addition, an adjacency list is used to store the node indices of each edge column-wise, resulting in a matrix of size $2 \times E$.

The labels consist of the three principal stresses $(\sigma_x, \sigma_y, \sigma_z)$ and the three shear stress components $(\tau_{xy}, \tau_{yz}, \tau_{xz})$, from which the von Mises stress can be computed. Since the loading conditions and material properties are identical across all FEM simulations, these quantities are not included as input features, as they do not provide additional information for the learning task.

Furthermore, the FEM meshes are inspected to ensure adequate mesh quality, and the dataset is analysed for potential bias. A uniform distribution of notch stresses is desired to avoid bias in the prediction performance of the trained models.

4.2. *Evaluation metrics*

It is common practice to compute an error or evaluation metric over all nodes of the mesh. Studies have already attempted to introduce metrics that are easy to interpret and well comparable (Jin et al. 2023; Shivaditya 2023). However, they do not allow for a meaningful assessment of the prediction quality of notch stresses. This is because, in most applications, the nodes associated with notch stresses constitute only a small fraction of the total number of nodes. For the butt weld configuration considered in this study, these nodes account for approximately 0.5% of all nodes. Consequently, their contribution to a global error metric is insufficient and is often overshadowed by other sources of error.

For this reason, both global and local evaluation metrics are employed. While the global metrics assess the overall prediction performance across the entire mesh, the local metrics specifically target the accuracy of notch stress predictions. To this end, for both weld toes (left and right), all nodes located in the corresponding weld toe region are selected for which Eq.(1) holds. Specifically, the stress at a node must lie within 0.05 MPa of the maximum von Mises stress in the respective weld toe region to be considered for the respective set of nodes *l* or *r*, where *l* and *r* denote the left and right side.

$$\sigma_i > \sigma_{max} - 0.05\ MPa \tag{1}$$

From the node sets l and r, the metrics MRE_{max} and STD_{max} are subsequently computed (see Eq.(2) - (3)). The metric MRE_{max} quantifies the absolute mean relative error (MRE) of the predicted notch stresses in percent, while STD_{max} represents the standard deviation of the stresses within the selected node sets. σ_{VM} are the real von Mises stresses and $\hat{\sigma}_{VM}$ are the predicted ones. The introduced metrics are easy to interpret and are well suited for application across different stress levels.

$$MRE_{max} = \frac{1}{2}\left(\frac{1}{l}\sum_{i=1}^{l}\frac{|\sigma_{VM,i}-\hat{\sigma}_{VM,i}|}{|\sigma_{VM,i}|} + \frac{1}{r}\sum_{i=1}^{r}\frac{|\sigma_{VM,i}-\hat{\sigma}_{VM,i}|}{|\sigma_{VM,i}|}\right)100\% \tag{2}$$

$$STD_{max} = \frac{1}{2}(STD_l + STD_r) \tag{3}$$

To evaluate the overall prediction performance across all nodes, the coefficient of determination R^2 is used (See Eq.(4)). An R^2 value of 1 indicates perfect predictive performance, whereas a value of 0 signifies no explanatory power.

$$R^2 = 1 - \frac{\frac{1}{N}\sum_{i=1}^{N}\left(\sigma_{VM,i} - \hat{\sigma}_{VM,i}\right)^2}{\frac{1}{N}\sum_{i=1}^{N}\left(\sigma_{VM,i} - \bar{\hat{\sigma}}_{VM}\right)^2} \tag{4}$$

4.3.*Architecture*

The GNNs employ an encoder–processor–decoder architecture, which is commonly used for stress prediction tasks in graph neural networks. A schematic overview of the workflow is shown in Fig. 2. PyTorch Geometric was used for the implementation, as it is one of the most widely adopted libraries for graph neural networks. The encoders transform the node and edge features into the hidden dimension h, which is subsequently used throughout the processor. Both the encoder and decoder are implemented as multilayer perceptrons (MLPs). Each MLP consists of a linear layer followed by a ReLU activation, a second linear layer, and a normalization layer. The decoder differs from the encoder in that it does not employ a normalization layer.

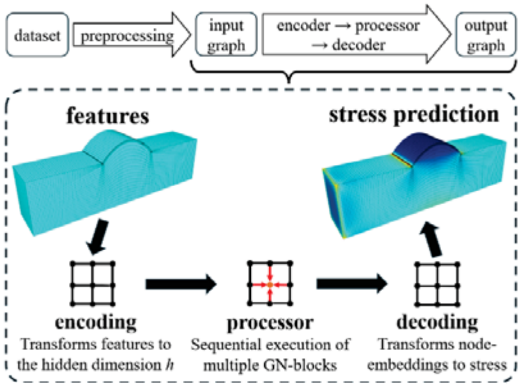

Fig. 2. Schematic overview of the GNN with an encoder-processor-decoder architecture and sequential execution of GN-Blocks.

The processor consists of a sequence of several identical GN blocks (Battaglia et al. 2018). Each GN-block consists of three main steps. First, during the message-passing phase, edge features are updated using an MLP_{edges} based on the edge embeddings e_{ij} and the embeddings of the sending nodes n_i and receiving nodes n_j. Second, the updated messages e'_{ij} are aggregated by summation for each node. Finally, the node embeddings are updated using an MLP_{nodes} that takes the aggregated messages $m_{\mathcal{H}(i)}$ and the current node embeddings v_i as input (See Eq.(5) - (7)) (Battaglia et al. 2018).

$$e'_{ij} = MLP_{edges}\left(e_{ij}, n_i, n_j\right) \tag{5}$$

$$m_{\mathcal{H}(i)} = \sum_{i,\forall j \in \mathcal{H}(i)} e'_{ij} \tag{6}$$

$$n'_i = MLP_{nodes}(m_{\mathcal{H}(i)}, n_i,) \tag{7}$$

The MLPs used for the update operations consist of a linear layer, a ReLU activation function, a second linear layer, and a normalization layer.
To reduce oversmoothing effects, concatenation was employed (Hamilton et al. 2020). As

regularization techniques, weight decay within the optimization procedure and edge dropout were applied, using typical values of 0.005 and 5%, respectively. Model optimization was performed using the Adam optimizer with a learning rate of 0.001.

The two most influential hyperparameters, the hidden dimension and the number of GN-blocks, showed strong performance when set within the ranges of 20 to 50 and 10 to 30, respectively. Larger models provided only marginal performance improvements while requiring higher training times.

4.4. *Physics informed loss*

Previous studies have combined GNNs with physics-informed loss formulations based on the principle of minimum potential energy and boundary conditions such as Dirichlet and Neumann constraints (Dalton et al. 2023; Zhou et al. 2024). In contrast, this study investigates a simpler and computationally less expensive approach. Rather than employing a fully physics-based formulation, a conventional loss function is augmented with selected physics-informed neural network (PINN) terms.

The baseline loss is defined as a mean squared error (MSE) computed over all nodes of the mesh. In addition, two PINN-based terms are introduced that specifically target the accurate prediction of notch stresses. The first term, denoted as $PINN_{sym}$, accounts for the symmetry condition of the welded joint. For the considered loading case, the notch stresses at the left and right weld toes are identical. Thus, any discrepancy between these values therefore indicates a non-physical model response. To obtain representative notch stress values, the average of the highest stress values within each weld toe region is computed. The second term, referred to as $PINN_{max}$, computes an additional MSE over a subset of nodes m exhibiting high stress levels in the weld toe region. This term penalizes models that exhibit poor accuracy in predicting notch stresses. The selection of the node set m follows a procedure similar to that described in Eq. (1), with a stress threshold of 0.15 MPa relative to the local maximum stress (See Eq. (8) - (11)).

$$Loss = MSE_{normal} + \beta(PINN_{sym} + PINN_{max}) \quad (8)$$

$$MSE_{normal} = \frac{1}{N}\sum_{i=1}^{N}\left(\sigma_{VM,i} - \hat{\sigma}_{VM,i}\right)^2 \quad (9)$$

$$PINN_{sym} = \left(\bar{\sigma}_{VM,left} - \bar{\sigma}_{VM,right}\right)^2 \quad (10)$$

$$PINN_{max} = \frac{1}{m}\sum_{i=1}^{m}\left(\sigma_{VM,i} - \hat{\sigma}_{VM,i}\right)^2 \quad (11)$$

σ_{VM} are the real von Mises stresses and $\hat{\sigma}_{VM}$ are the predicted ones. The influence of the PINN-based terms is controlled by a weighting factor β.

4.5. *Training procedure*

The models were trained on an NVIDIA RTX 5500 GPU and an early stopping strategy was employed. Model convergence was typically achieved after 386 ± 84, with training times of 100 ± 65 minutes, depending on the specfics parameter configuration (mean $\pm$ standard deviation). Training was performed in batches, using batch sizes ranging form 3 to 5. The training behaivor was consistent with that typically observed in deep learning models. A train-test-splot of 4:1 was used.

5. Results

5.1. *Comparison basic GNN and modified GNN*

In this section, the best-performing baseline GNN, which uses only MSE_{normal}, is compared with the best-performing modified GNN that additionally incorporates both PINN-based terms. Table 2 summarizes the evaluation metrics introduced in Section 3.2 for the respective models.

Table 2: Evaluation metrics of the best baseline and modified GNN. (mean $\pm$ standard deviation)

Metric	Baseline GNN	Modified GNN
R^2 [−]	0.976±0.019	0.970±0.019
MRE_{max} [%]	3.57±2.81	2.75±1.75
STD_{max} [−]	0.0484±0.0211	0.0281±0.0193

The modified GNN achieves more accurate predictions of notch stresses in the weld toe region, as reflected by a lower $\mathrm{MRE}_{\max}$ value and a reduced associated variability. Moreover, the variability of the predicted stresses within the node set relevant to notch stress evaluation is reduced, as reflected by the lower $\mathrm{STD}_{\max}$. This indicates that the modified GNN is able to identify the nodes at which maximum stresses occur better. In contrast, the overall prediction performance, expressed by the coefficient of determination R^2, is slightly lower for the modified GNN compared to the baseline model. With respect to the global prediction variance, both architectures exhibit similar characteristics.

However, the employed evaluation metrics do not allow for a geometric assessment of the predictions, which is only possible through 3D-visualizations. Such visualizations are limited in that they can represent only a single geometry at a time. To address this limitation, a normalized weld toe representation is introduced (see Fig.3).

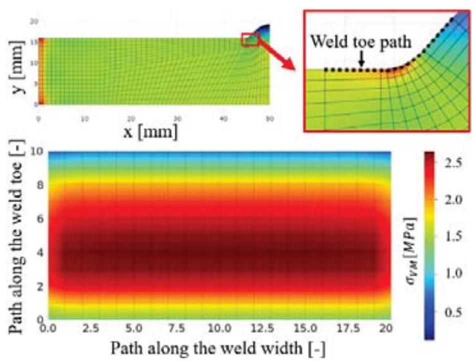

Fig. 3. Illustration of the path along the weld toe (top). Visualization of the von Mises stresses in the normalized weld toe geometry (bottom).

For this purpose, the nodes along the weld toe are unwrapped across the width of the weld. This procedure allows the weld toes of all welded joints to be mapped onto a standardized 21×11 matrix, making the stress distribution along the weld toe more clearly visible and enabling straightforward evaluation and comparison across multiple predictions

Figure 4 shows the MRE over the entire test dataset for the GNN models listed in Table 2. In contrast to the computation of MRE_{max}, the absolute value is not taken prior to the MRE calculation in this case, which leads to differing values.

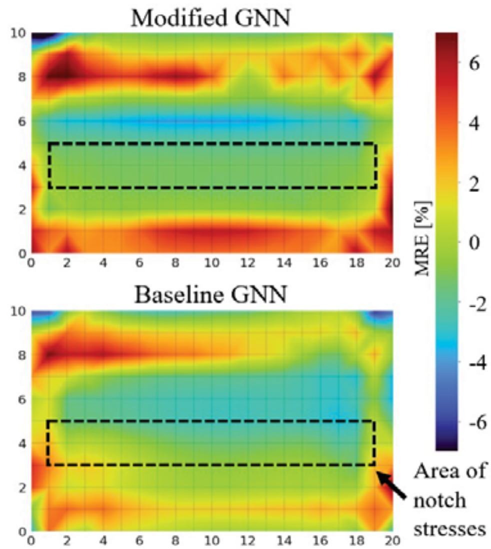

Fig. 4. Normalized weld toe representation (See Fig.3) for the GNNs shown in Table 2. MRE over the entire test dataset.

In the region of the notch stresses, the modified GNN exhibits a lower deviation and reduced dispersion among the nodes in this area. Outside the notch stress region, the modified GNN is less accurate than the baseline GNN. Overall, this observation is consistent with the findings derived from the evaluation metrics presented in Table 2 and further demonstrates the usefulness of the proposed evaluation metrics for the evaluation of notch stresses.

5.2. Generalization

To assess the generalization capability of the proposed models, a fillet weld configuration is introduced. The fillet weld is fully penetrated, and the FEM meshing is performed in accordance with the notch stress approach (DVS 0905, 2021). The loading conditions are identical for all FEM simulations, with only the geometry being varied. Fig. 5 shows the side view, which was extruded by 20 mm to generate the three-dimensional geometry. The value ranges are displayed in Table 3.

Table 3: Value ranges of the geometry parameters for the FEM-Simulations for the fillet weld geometry.

Geometry parameter	Value range
Reference radius r	0.3 – 1.5 mm
Plate thickness t	5 – 15 mm
Opening angle α	30 – 60 deg

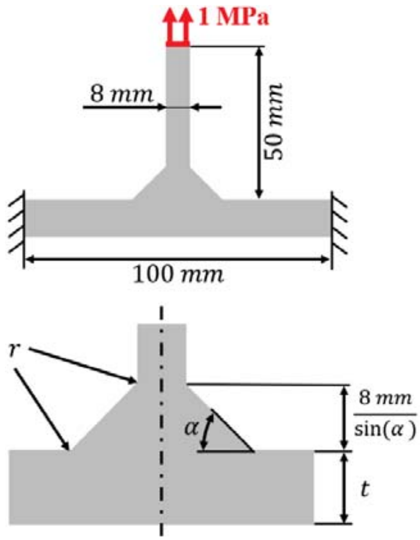

Fig. 3: Loading condition and geometry parameters for the fillet weld geometry.

First, the GNN models listed in Table 2 were evaluated on a dataset consisting of fillet welds. The results are poor, with negative R^2 values ranging between −0.3 and −0.4. This indicates that the GNN architecture cannot generalize from butt-weld structures to fillet-weld structures.

In a subsequent step, a new dataset was generated comprising an equal proportion of butt welds and fillet welds. The dataset contains a total of 396 FEM simulations. Table 4 summarizes the best results obtained for both architectures when trained on this combined dataset.

Table 4: Evaluation metrics of the best baseline and modified GNN trained on both weld geometries. (mean $\pm$ standard deviation)

Metric	Baseline GNN	Modified GNN
R^2 [−]	0.641±0.572	0.636±0.496
MRE_{max} [%]	10.21±3.99	4.62±1.67
STD_{max} [−]	0.180±0.076	0.072±0.046

The prediction performance is lower than in the case where training and testing are performed on a single weld configuration. However, the trained GNNs are now able to provide meaningful predictions for both weld geometries. The overall prediction performance is substantially reduced (R^2), which is primarily attributable to the fillet welds. These exhibit a more complex stress field, and variations in the plate thickness t lead to changes in the ratio between nodes that are easy and difficult to predict. As a result, very low R^2 values are obtained for the fillet welds for both architectures. For the modified GNN, R^2 values of 0.422 ± 0.630 are achieved for fillet welds and 0.85 ± 0.081 for butt welds. A similar behavior is observed for the baseline GNN. This demonstrates that the R^2 metric is only of limited suitability in this context. In contrast, the metrics MRE_{max} and STD_{max} remain robust and informative. Here, the modified GNN again clearly demonstrates its advantages, achieving approximately a factor of two improvements in accuracy compared to the baseline GNN, along with a significantly reduced prediction variability.

6. Conclusion

In this work, FEM-based datasets for welded structures with butt and fillet welds were generated using an automated workflow and used to train GNNs for stress prediction. A baseline GNN was extended by incorporating physics-informed terms into the loss function, which improved the prediction accuracy of notch stresses at the weld transition. In addition, specialized evaluation metrics and a normalized weld transition representation were introduced to enable spatially resolved comparison of model performance in critical stress regions.

The integration of PINN-terms enhanced the prediction of notch stresses but slightly reduced the global prediction accuracy. Furthermore, the results indicate that GNNs exhibit limited generalization to geometries that deviate significantly from the training data. Training on multiple structures improves generalization but reduces accuracy compared to structure-specific models. Nevertheless, the PINN-based approach consistently improved the prediction of critical stresses, independent of the geometry.

Overall, GNNs represent a promising approach for stress prediction in welded structures, but their applicability strongly depends on the availability of representative training data, and their flexibility remains limited compared to conventional numerical methods.

Building on the results of this work, several directions for future research can be identified. Restricting the training of the GNN to datasets with a unified reference radius, would lead to more consistent stress fields and improved prediction accuracy. Moreover, improved mesh quality and smoother transitions in the weld region are expected to positively affect both FEM accuracy and surrogate model performance, motivating further investigation.

In addition, future studies should address the generalization capability of the GNN with respect to varying load cases, boundary conditions, materials, and welding-related effects such as heat-affected zones, which could be incorporated via suitable node or edge features. Finally, a more general formulation of the PINNs and the adoption of relative error measures could enhance robustness and transferability across structures with varying stress magnitudes.

References

Hamilton, W. L. (2020). *Graph Representation Learning*.

Kim, N.-H., Sankar, B. V., & Kumar, A. V. (2018). *Introduction to Finite Element Analysis and Design*. Wiley & Sons Ltd.

Herrmann, L. and Kollmannsberger, S. (2024). Deep learning in computational mechanics: a review. *Computational Mechanics 74*.

Shivaditya, M. V., Alves, J., and Buigotti, F. (2023). Graph neural network-based surrogate models for finite element analysis, *DCABES*.

Wong, J. C., Ooi, C. C., Chatoraj, J., Lestandi, L., and Dong, G. (2023). Graph neural network based surrogate model of physics simulations for geometry design. *IEEE Access 11*.

Wu, J., Du, C., Dillenburger, B., & Kraus, M. A. (2024). Fast prediction of stress distribution: a GNN-based surrogate model for unstructured mesh FEA. *IASS*.

Jelovica, J., & Cai, Y. (2025). Graph neural network for stress predictions in stiffened panels. *Journal of Maritime & Transportation Sciences Special Edition No.5*, 243-252.

Xia, F., Shi, G., Gao, Z., Li, J., Xu, S., & Ruan, D. (2025). Predicting deformation and stress-strain behaviour of lattice truss structures under compression using dual Graph Neural Network. *Composite Structures 312*.

Yang, Y., Hong, X., & Liu, N. (2025). Graph neural network-based three-dimensional stress prediction. *ICIEIS 2024*.

Jin, Z., Theng, B., & Kim, C. (2023). Leveraging graph neural networks and neural operator techniques for high-fidelity mesh-based physics simulations. *APL Machine Learning 1*.

Dalton, D., Husmeier, D., & Gao, H. (2023). Physics-informed graph neural network emulation of soft-tissue. *Computer Methods in Applied Mechanics and Engineering 417*.

Feng, B., & Zhou, X. (2024). Energy-informed graph transformer model for solid mechanical analyses. *Communications in Nonlinear Science and Numerical Simulation 137*.

Gulakala, R., Market, B., & Stoffel, M. (2022). Graph neural network enhanced finite element modelling. *PAMM 22(1)*.

Pfaff, T., Fortunato, M., Gonzalez, A. S., & Battaglia, P. W. (2021). Learning mesh-based simulation with graph networks. *ICLR 2021*.

Zhou, J., Cui, G., & Hu, S. (2020). Graph neural networks: a review of methods and applications. *AI Open 1*.

Battaglia, P. W., Hamrick, J. B., & Bapst, V. (2018). Relational inductive biases, deep learning, and graph networks. *arXivPpreprint.*

DVS Verband (2021). *Merkblatt DVS 0905*. Düsseldorf: DVS Verband.